REPORT DOCUMENTATION PAGE

Form Approved
OMB NO. 0704-0188

1. AGENCY USE ONLY (Leave Blank)	2. REPORT DATE	3. REPORT TYPE AND DATES COVERED
	March 18, 2004	**Final 3/19/2001 – 09/30/2003**

4. TITLE AND SUBTITLE
Direct Numerial Simulation of Turbulent Drag Reduction: Molecular Modeling, Molecular Optimization, and Modeling without Consititutive Equations.

5. FUNDING NUMBERS
MDA972-01-C-0041

6. AUTHOR(S)
E.S.G. Shaqfeh, P. Moin, S. Lele, Y. Dubief and C. Dimitropoulos

7. PERFORMING ORGANIZATION NAME(S) AND ADDRESS(ES)
Stanford University
Mechanical Engineering Department
Flow Physics and Computation Division, Stanford, CA 94305-3030

8. PERFORMING ORGANIZATION REPORT NUMBER

9. SPONSORING / MONITORING AGENCY NAME(S) AND ADDRESS(ES)
Defense Advanced Research Projects Agency (DARPA)
Advance Technology Office
Attn: Dr. Lisa Porter
3701 North Fairfax Drive
Arlington, VA 22203-1714

10. SPONSORING / MONITORING AGENCY REPORT NUMBER

11. SUPPLEMENTARY NOTES
The views, opinions and/or findings contained in this report are those of the author(s) and should not be construed as an official Department of the Army position, policy or decision, unless so designated by other documentation.

12 a. DISTRIBUTION / AVAILABILITY STATEMENT
Approved for public release; distribution unlimited.

12 b. DISTRIBUTION CODE

13. ABSTRACT (Maximum 200 words)

We present numerical simulations of turbulent drag reduction in wall-bounded flows by additives. The bulk of the work concentrates on polymer additives. A multiscale approach was used to study the fine details of polymer dynamics in turbulence and the transfer of energy between polymers and turbulence. It was shown that polymers extract energy from near-wall vortices and release energy in high-speed streaks very close to the wall. We derived a conceptual model which applies to the two, statistically distinct regimes of polymer drag reduction, namely low drag reduction (LDR) and high drag reduction (HDR). Another additive, fibres, was found to obey to a different mechanism which requires close interaction of mutiple vortices.

14. SUBJECT TERMS	15. NUMBER OF PAGES
Drag reduction, Polymer addition, turbulent boundary layer, low drag reduction, high drag reduction	**20**
	16. PRICE CODE

17. SECURITY CLASSIFICATION OR REPORT	18. SECURITY CLASSIFICATION ON THIS PAGE	19. SECURITY CLASSIFICATION OF ABSTRACT	20. LIMITATION OF ABSTRACT
UNCLASSIFIED	**UNCLASSIFIED**	**UNCLASSIFIED**	**UL**

NSN 7540-01-280-5500

Standard Form 298 (Rev.2-89)
Prescribed by ANSI Std. 239-18
298-102

20040331 040

Enclosure 1

Final Technical Report

Direct Numerial Simulation of Turbulent Drag Reduction: Molecular Modeling, Molecular Optimization, and Modeling without Consititutive Equations

E.S.G. Shaqfeh, P. Moin, S. Lele, Y. Dubief and C. Dimitropoulos
Stanford University
Stanford, CA 94305

Sponsored by:
Defense Advanced Research Project Agency (DARPA)
Advanced Technology Office
Friction Drag Reduction Program
ARPA Order No. K042/31, K042/13
Issued by DARPA/CMO under Contract No. MDA972-01-C-0041

1 Task Objects

Drag reduction using polymer additives in wall-bounded flows poses many challenges to our understanding of turbulence and polymer dynamics. Up to 80% of friction-drag reduction can be obtained with ultra dilute solutions of high molecular weight polymers, for which each molecule is several orders of magnitude smaller than the smallest turbulent scale of the flow. To investigate this multiscale problem, numerical simulations at the microscopic and macroscopic level were performed. At the microscopic level, Brownian dynamics (BD) simulations were used to assess the realism of polymer models and to document the effect of turbulence on polymer configuration. Drag reduced flows were investigated using direct numerical simulations (DNS) of viscoelastic flow (macroscopic simulation). DNS was able to show how energy is transferred between turbulent structures and polymers in turbulent channel flow and boundary layers. It also allowed for the detailed investigation of the two different regimes of polymer drag reduction, namely low drag reduction (LDR) and high drag reduction (HDR). Based on the DNS and BD results, a model for the mechanism of polymer drag reduction has been proposed. The DNS formalism was also extended to fibres additives for which a model of the mechanism of drag reduction was also derived.

2 Technical problem

BD and DNS were solved using state of the art flow solvers developed at Stanford. The challenge of the BD simulation was to implement an efficient and reliable particle tracking technique in a fully parallelized code. The DNS of viscoelastic flow had to overcome small-scale instabilities arising from the resolution of the macroscopic polymer model. Both of these problems were solved adequately as is described in the Technical Results section.

3 General Methodology

The addition of small amounts of long chain polymer molecules to wall-bounded flows can lead to dramatic drag reduction. Although this phenomenon has been known for about fifty years, the action of the polymers and its effect on turbulent structures are still unclear. Detailed experiments have characterized two distinct regimes (Warholic *et al.*, 1999), which are referred to as low drag reduction (LDR) and high drag reduction (HDR). The first regime exhibits similar statistical trends as Newtonian flow: the log-law region of the mean velocity profile remains parallel to that of the Newtonian flow but its lower bound moves away from the wall and the upward shift of the log-region is a function of drag reduction, herein referred to as DR. Although streamwise fluctuations are increased and transverse ones are reduced, the shape of the rms velocity profiles is similar. At higher drag reductions, larger than about 40%, the flow enters the HDR regime for which the slope of the log-law is dramatically augmented and the Reynolds shear stress is small (Warholic *et al.*, 1999; Ptasinski *et al.*, 2003). The drag reduction is eventually bounded by a maximum drag reduction (MDR, Virk & Mickley, 1970) which is a function of the Reynolds number.

In drag reduced flows, a stress deficit is observed in the stress balance whose large magnitude at HDR has been interpreted as the necessary input of energy from the polymers to the flow for the sustenance of the asymptotic MDR turbulence (Warholic *et al.*, 1999). Recently, numerical simulations have allowed the simultaneous study of velocity and polymer fields, giving the opportunity to relate turbulence and polymer stress directly. Several explanations have been proposed for the mechanism of polymer drag reduction through such computations. Based on averaged budgets of kinetic and energy, Dimitropoulos *et al.* (2001) observed that streamwise enstrophy is inhibited by the extensional viscosity generated by polymers stretched by turbulence. Based on a similar argument, Ptasinski *et al.* (2003) related the damping of vortices to a shear sheltering effect occurring in the near-wall region which would effectively decouple the outer layer vortices from the inner layer. Neither paper proposes a

mechanism for the injection of energy from polymers to turbulence. Min *et al.* (2003*b*,*a*) analyzed their simulation in terms of elastic energy, observing that a significant transport of this energy from the viscous sublayer to the buffer layer and the log region. They derived a criterion of the onset of drag reduction based on the relaxation time and the time required for polymers to travel from the viscous sublayer to the buffer layer. These authors explain MDR by the release of energy into the buffer layer, which would be sufficient to sustain turbulence.

All the studies referenced above have relied on DNS of turbulent channel flow and conclusions were derived from time and space averaged statistics. Such statistics can hide important intermittent events. Due to the intermittent character of near-wall turbulence, our effort focused on the accurate computation of small scale events and their characterizations in terms of coherence and relation to turbulent structures. BD using advanced polymer models was used for the first time in turbulent channel flows, providing insights on the dynamics, while DNS was able to document local transfer of energy between polymers and turbulence. This combined effort led to a model of polymer drag reduction which describes how turbulent energy is stored by polymers and where this energy is released, for both LDR and HDR regimes. Simulations of turbulent boundary layers were developed for comparison with the Stanford experiment in Phase II of the Friction Drag Reduction project. Finally, DNS of fibre additives highlighted a different mechanism of drag reduction.

3.1 Polymer models

All the models tested here are derived from the Finitely Extensible Non-linear Elastic (FENE) model. Different levels of refinement were tested using BD simulations, while DNS was performed using the FENE-P model only.

3.1.1 FENE

The FENE model is based on an elastic dumbbell which represents the polymer molecule as two beads connected by a spring Bird *et al.* (1987); Herrchen & Oettinger (1997). The non-linear spring force is modeled by a Warner spring representing the entropic forces which tend to bring the polymer back into its coil configuration. The non-linearity of the spring ensures that the dumbbell cannot extend more than a given maximum extensibility. The equation for the extension of the polymer is derived by neglecting the inertia of the beads and equilibrating the different forces acting on the beads. Polymer molecules (microscopic model) or solutions (macroscopic or constitutive model) are defined by the polymer relaxation time (Weissenberg number We) and the maximum length of a polymer molecule L. In the case of a polymer solution, β, the ratio of the solvent viscosity ν to the total viscosity, effectively controls the concentration of polymers.

3.1.2 FENE-P

The FENE-P model (P for Perterlin) describes the ensemble average evolution of polymer configuration, assuming homogeneous concentration. The FENE-P model is therefore macroscopic and generally described in the Eulerian framework. BD simulations using this model were also performed to compare Eulerian and Lagrangian advection of polymer quantities.

3.1.3 FENE-P Brownian

This model is hybrid FENE/FENE-P model, where the average polymer configuration is computed using FENE-P but the model still has the stochastic Brownian term.

3.1.4 FENE MULTICHAIN

The FENE multichain model It consists of a chain of beads connected by springs. The derivation of the equation for the end-to-end vectors is similar to that of the FENE dumbbell

Somasi *et al.* (2002*a*). The bead-spring chain is a less coarse approximation of a polymer molecule, since it takes account of some of the internal relaxation modes which are present in a real molecule.

3.1.5 Fibres model

Drag reduction induced by rigid fibres in a turbulent channel flow using direct numerical simulation were investigated using the channel flow code developed for polymer drag reduction. The fibres are modeled using a well-known constitutive equation involving the moments of orientation vector and two closure approximations (Hinch & Leal, 1976). The model has a form similar to the constitutive FENE-P model.

3.2 Flow solver

The flow solver is based on robust finite difference schemes which allow for the simulation of complex geometries. The code, based on Pierce (2001), utilizes a staggered grid and second-order finite differences for spatial derivatives. Time integration is semi-implicit, using either a third order Runge-Kutta/ Crank Nicolson scheme Dubief (2002) or an iterative method developed by Pierce (2001) to enhance secondary conservation and nonlinear stability. Similar codes have been extensively used and validated at the Center for Turbulence Research for a wide variety of problems including combustion and particle-laden flows.

3.3 Particle tracking

For BD simulations, polymer trajectories are solved using Lagrangian advection. The integration of the polymer molecule trajectories assumes that the molecule center-of-mass motion is characterized by no inertia and an infinite Peclet number. Therefore, these trajectories represent an exact Lagrangian description of the flow. To accommodate the small scale behavior of polymers, the trajectories are integrated at a smaller time step than that of the flow. Therefore, the velocity at the intermediate time steps is obtained by linearly interpolating two flow fields in time. The polymer molecule itself is advanced using a second order Runge–Kutta scheme. Since the Eulerian velocity is only known on a grid network, a spatial interpolation is needed to determine the velocity at its current position. The trilinear interpolation was found to be sufficient (Terrapon *et al.*, 2003). The time integration of FENE models uses a semi-implicit predictor-corrector scheme (Oettinger, 1996; Somasi *et al.*, 2002*b*)

3.4 DNS of viscoelastic flows

The FENE-P model in the Eulerian framework leads to the calculation of polymer stress which enters the Navier Stokes equations as an extra term. The numerical solution of the FENE-P model requires high order methods as pointed out by Min *et al.* (2001). To capture the small scales generated by the model, some derivatives have to be calculated using compact schemes Dubief (2002), as is discussed in the Technical Results section.

3.5 Flow description

3.5.1 Channel flow

The channel flow domain assumes periodicity in directions parallel to walls, streamwise and spanwise. No-slip is prescribed on walls. Mass flow is kept constant so that drag reduction is measured as a drop in streamwise pressure gradient.

DNS simulations are performed at an intermediate Reynolds number, $Re_c = 7500$, or a bulk Reynolds number of $Re_M = 5000$. Conservation of the mass flow is imposed which gives $h^+ = hu_\tau/\nu = 300$, where h is the channel half width, $u_\tau = \sqrt{\nu(d\overline{U}_x/dy)_{wall}}$ is the friction

velocity and ν is the kinematic viscosity. The superscript $^+$ indicates quantities normalized by u_τ and ν. The resolution is $\Delta x^+ = 9$, $\Delta y^+ = 0.1 - 5$ and $\Delta z^+ = 6$, when normalized by the skin friction at DR=0%. The polymer parameters used in the course of this study are shown in Table 1. The streamwise and spanwise dimensions and resolutions were adjusted to accommodate highly drag reduced flows which length scales grow significantly. According to the Stanford experiment, the streamwise coherence of the streaks could be increased by an order of magnitude of the Newtonian length scale $l^+ \sim 1000$. In a preliminary parametric study for 60% of drag reduction, streamwise correlations of velocity were indeed found to be small yet finite even for $L_x^+ = 6000$ based on the Newtonian friction velocity, while $L_z^+ = 1000$ proved to be sufficient. Decreasing L_x^+ to 4000 had a negligible impact on the magnitude of drag reduction, less that 5% well within the convergence error of statistics, and this length was adopted for the present study. The dimensions of the computational domain is thus $4\pi h \times 2h \times 4h$.

For BD simulations, the computational domain is reduced to a minimal channel flow (Jiménez & Moin, 1991) of dimensions $\pi h \times 2h \times h$. The simulation has been carried out on a grid of $96 \times 151 \times 64$ points so that $dx^+ = 9.5$, $dy^+ = 0.2 - 10$ and $dz^+ = 4.5$. Finally a constant time step of $dt = 0.01H/U$ was chosen, ensuring a maximum $CFL = 0.6$. To achieve converged statistics, a large ensemble of particles are needed. In this case $N = 10^5$ particles were used with each of them having a different trajectory. The extensibility parameter was chosen to be $= L^2 b = 3600$ in order to simulate real molecules. Calculations were also performed for $b = 900$ and $b = 10000$, which gave qualitatively the same results. The bead-spring chain used had 5 springs corresponding to 5 relaxation modes. In all simulations we used a Weissenberg number $We = 3$ corresponding to a Weissenberg number based on the wall shear $We^+ = \frac{\lambda_H u_\tau}{\nu} = 34$. The equations for the polymer molecules were advanced using a time step $dt_p = 0.001$ which was ten times smaller than that of the flow calculation.

3.5.2 Boundary layer

For the momentum equations, the inflow, outflow and free-stream boundary conditions are very important given that they are approximate and not trivial. For the outflow, the convective condition is used (see the discussion in Na, 1996). For the free-stream, the zero vorticity condition is applied for the streamwise velocity, u, the zero shear constraint for the spanwise velocity, w and the outflow velocity, v, is consistent with the boundary layer growth, through on the fly computation of an integral scale (displacement thickness) (Na, 1996; Lund *et al.*, 1998; Jacobs & Durbin, 2001):

No slip and periodic conditions are used in the spanwise direction and on the wall. The inflow condition is supplied from a Newtonian simulation which uses an inflow profile constructed by recycling from a downstream station, using the approach of Lund *et al.* (1998). The recycling method of Lund has been proven to minimize errors at the inflow due to flow readjustment. Alternatively, one can use recycling in conjunction with a freely developing inflow conformation profile.

Several simulations of viscoelastic turbulent boundary layer flow with the FENE-P model have been performed recently in order to validate the method. The first simulations were for uncoupled flow at a maximum extension L^2 of 900 and a Weissenberg number (based on the Newtonian inflow shear rate at the wall), We_τ, equal to 25. The coupled simulations were first at the extensibility and elasticity values described above and then at $L^2 = 3600$ and $We_\tau = 50$. The Reynolds number, Re_θ, considered so far is relatively low, equal to 300 when based on the inlet momentum thickness. This was motivated by the desire to minimize the computational cost of the first cases studied in order to facilitate the development and validation of the algorithm. At these parameter values a grid of $128 \times 65 \times 128$ in the streamwise, x, wall-normal, y, and spanwise, z, direction is adequate (Na, 1996). The size of the computational domain was equal to $87\delta_{in}^* \times 19\delta_{in}^* \times 25\delta_{in}$, where δ_{in} is the displacement thickness at the inflow boundary. The spatial resolution in wall units (calculated with the inlet friction velocity) is in all cases $\Delta x^+ = 18.4$, $\Delta y^+ = (0.17 - 27)$ (a hyperbolic tangent

stretching function is used) and $\Delta z^+ = 5.3$.

3.6 Technical results

3.7 Brownian dynamics

For this project, our first approach was to compare the different polymer models. Figure 1 shows the mean and RMS of the square extension $\hat{Q}^2$ non-dimensionalized by the maximum extensibility parameter b as a function of the distance to the wall y^+. The square extension Q^2 of the polymer is defined as the norm square of the extension vector $\mathbf{Q}$. For the constitutive FENE-P model, it is defined as the trace $\langle Q_i Q_i \rangle$ of the conformation tensor. It can be seen that all models give qualitatively the same profile. However, the FENE and MULTICHAIN models have a slightly lower mean extension. The RMS are similar for all models except for the Brownian FENE-P, which has much higher fluctuations. A comparison of the different models along the same trajectory is presented in Fig. 2 (note that the initial conditions were different). The behavior of the different models is again qualitatively similar, even if each particle has a different stretch history.

To investigate the dynamics of polymer in turbulence, the evolution of polymer stretch was found to correlate to that of eigenvalues and invariants of the velocity gradient (Chong *et al.*, 1990). For an incompressible flow the eigenvalues, σ, are obtained as solutions of the characteristic equation

$$\sigma^3 + Q\sigma + R = 0, \tag{1}$$

with the tensor invariants Q and R given by

$$Q = -1/2\mathrm{tr}\left((\nabla \boldsymbol{u})^2\right), \tag{2}$$

$$R = -\det(\nabla \boldsymbol{u}). \tag{3}$$

The nature of the eigenvalues is determined by the discriminant $D = (27/4)R^2 + Q^3$. $D > 0$ gives rise to one real, two complex-conjugate eigenvalues; $D < 0$ gives three real distinct eigenvalues and $D = 0$ corresponds to three real eigenvalues of which two are equal.

Following this approach, it was shown that regions of the flow where $D > 0$ and $R > 0$ in a (Q, R) plot (implying a negative real eigenvalue and two complex-conjugate eigenvalues with positive real parts) unravel the polymer molecule at a sufficient high Weissenberg number. In this particular case, the stretching does not occur along a specific direction but along a rotating axis in the plane associated with the complex-conjugate eigenvalues. This shows that the stretching of the polymer is driven by the extensional character of the flow quantified by the positive real part of the eigenvalues. From this topological analysis, one can conclude that a polymer molecule will only fully unravel if it experiences a flow with a strong extensional character, i.e., one of the eigenvalues of the local velocity gradient tensor has a large positive real part. Therefore, we introduce

$$\sigma^* \equiv \max_i \left(\mathrm{Re}(\sigma_i)\right). \tag{4}$$

as a measure of the ability of the flow to stretch the polymer molecule.

In Fig. 3 shows the history of σ^*, Q and R that particles experiences before they reach significant extensions. The plots are obtained by conditional sampling based on the extension of polymers. At low We the polymer molecules experience a burst in σ^* just before reaching the threshold value. When We is increased, the maximum value of σ^* decreases (see figure 3 *a*). Figure 3 (*d*) illustrates that even at a larger We a large σ^* is needed to extend the polymer near to its maximum extension.

Flow visualizations also demonstrated that the regions of large σ^* are always located next to the vortices and can also be seen as structures advected by the mean flow. This is illustrated in figure 4, which shows isosurfaces of Q representing the vortices, isosurfaces of σ^* and the polymer molecules which are highly stretched. The correlation between σ^* and the vortices is striking and can provide new insight into the mechanisms of polymer drag reduction.

3.8 DNS of channel flow

The stability of the constitutive equations was carefully investigated in Dubief *et al.* (2004*a*). Due to the lack of diffusion in the constitutive FENE-P model, the polymer configuration field tends to develop sharp gradient. As a consequence, an approach similar to that used for shocks is required or dissipation must be added to the model. We have tested the two approaches and demonstrated that adding a dissipative term to the model leads to a significant damping of polymer stress at small scales. Fig. 5 Since the drag reducing effect is significant at scales not much larger than the smallest flow scale, an upwind high-order scheme combined with local artificial dissipation was adopted (Dubief *et al.*, 2004*a*).

DNS in channel flows allowed the statistical characterization of LDR (low drag reduction) and HDR (high drag reduction) regimes, as shown in Figs. 6 and 7 (Dubief *et al.*, 2004*b*).

As expected from experiments (Warholic *et al.*, 1999), DR=35% produces a velocity profile whose log region is only shifted upward, while DR=47% and DR=60% show significant changes in the slope of the log law. Although we did not attempt to determine an accurate limiting value, the transition between LDR and HDR seems to be near 40% of drag reduction, in agreement with Warholic *et* al.'s measurements. The turbulent velocity fluctuations in the transverse directions exhibit a different behavior than in the streamwise direction. The peak of u'_x (a' denotes the root mean square of a fluctuations) shifts away from the wall and its magnitude increases slowly compared to the Newtonian flow when normalized by u_τ. The wall-normal component u'_y follows an opposite trend; u'_z behaves as u'_y and consequently does not appear on the plot for clarity. In drag reduced flow, the maximum of u'^+_x is higher or comparable with the DR=0% case, as found in experiments (Warholic *et al.*, 1999; Ptasinski *et al.*, 2003; White *et al.*, 2003*b*). The strong reduction of the transverse fluctuations suggests that polymers target preferentially the vortices, as they produce significant fluctuations of u_y and u_z.

The balance of shear stress,

$$-\overline{u_x u_y}^+ - \left(1 - \frac{y^+}{h^+}\right) + \beta \frac{dU_x^+}{dy^+} + (1-\beta) T_{xy}^+ = 0\,, \tag{5}$$

contains significant information regarding the mechanism of polymer interaction with the mean flow. In Eq. (5), T_{xy} is the average of $\tilde{\tau}_{xy}$. As indicated in Fig. 7, the Reynolds shear stress is reduced with increasing drag reduction. For DR=60%, $-\overline{u_x u_y}^+$ is approximately a third of its magnitude in the Newtonian case. Conversely, the polymer stress increases with increasing drag reduction. At DR=60%, its near-wall contribution to Eq. (5) has the same magnitude as the Reynolds shear stress, thus showing that polymers have a significant mean effect in the mechanism of HDR flows, as argued by Warholic *et al.* (1999).

To characterize the energy which is stored or released by polymers from each fluctuating velocity component, we consider the Reynolds stress equation (where summation does not apply to the subscript α)

$$\frac{1}{2}\partial_t u_\alpha^2 = \underbrace{(-u_\alpha \partial_j u_\alpha u_j)}_{A_\alpha} + \underbrace{(-u_\alpha \partial_\alpha) p}_{P_\alpha} + \underbrace{\frac{\beta}{Re} u_\alpha \partial_j \partial_j u_\alpha}_{V_\alpha} + \underbrace{\frac{1-\beta}{Re} u_\alpha \partial_j \tau_{\alpha j}}_{E_\alpha}\,. \tag{6}$$

The relation between polymers and turbulence enters through the *polymer work* E_α, product of the velocity and polymer body force, which could dampen ($E_\alpha < 0$) or enhance ($E_\alpha > 0$) the energy carried by velocity fluctuations u_α. The other terms denote work by advection A_α, pressure redistribution P_α and viscous stress V_α; the sum of these terms will be later referred as to Newtonian work.

By plotting the joint probability density functions of polymer work with other works, we were able to correlated negative polymer work (polymer storing turbulent energy) with upwash and downwash flows and positive polymer (polymer giving energy back to the flow) work with high speed streaks very close to the wall (see Fig. 8). The latter phenomenon

was found to occur in regions where viscous work dominates and tends to damp streamwise velocity fluctuations. By releasing their energy in these regions, polymers actually overcome viscous work and generates a growth of streamwise velocity fluctuations (Fig. 8). This transfer of energy from polymers to turbulence is responsible for preventing the flow from relaminarizing therefore plays a key role in MDR (maximum drag reduction).

3.9 DNS of boundary layer

The simulation of turbulent boundary layer started late in phase I and extends to phase II. Statistical results for the velocity (not shown here) are consistent with channel flow simulation. Here we present the coupled case with higher viscoelasticity which was thoroughly investigated for its interesting properties. After the stationary state in time was reached, averaging was performed over approximately 220 inertial time-units (4 flow-through times). The predicted drag reduction along the streamwise length of the plate exhibits initially a slight drag increase close to the inflow boundary, which evolves rapidly to a larger drag reduction, reaching 40% close to the outflow location, where a small region of constant drag reduction is observed (Fig. 9). In addition, the conformation shows that there is a larger region close to the inflow where stretching is most intense and that this causes more rapid damping of the vortices downstream. This results in weaker stretch downstream, which reaches a constant value close to the outflow of the current computational domain (Fig. 10). In addition, the concept of polymer stretch being clearly out of phase with its result on the flow field (for example, vortex intensity) is reinforced (Fig. 11). The evolution of the stretch of the polymer in these coupled simulations underlines the importance of direct numerical simulations of viscoelastic turbulent boundary layers because they capture the experimentally observed development region (White *et al.*, 2003*a*) even for the case where the polymer is modeled with assumption of homogeneous concentration. Channel flow simulations can only capture a spatially stationary region, which does not provide a complete understanding of the evolution of drag and microstructure that can be applied toward optimization of an injection experiment.

This work, its validation and preliminary results are available in an internal report Dimitropoulos *et al.* (2003).

3.10 Drag reduction with fibres

Drag reductions of up to 21% were calculated, with the largest drag reductions observed for non-Brownian rods at semi-dilute concentrations. These findings suggest that elasticity is not necessary in order to achieve Results and fibre parameters are reported in Paschkewitz *et al.* (2004).

The mean velocity and RMS velocity fluctuations for the Newtonian and drag-reduced cases are presented in figure 12. The fibre drag-reduced mean velocity profile was found to be similar to that observed in other drag-reduced flows, as for instance polymer flows: the slope of the log-law region is roughly the same as that of the Newtonian case, but the intercept with the linear region ($u^+ = y^+$) is shifted upwards. This log-law shift is indicative of a thickening of the viscous sublayer. The RMS velocity fluctuations are also qualitatively similar to those seen in polymeric simulations, with an increase and outward shift of the streamwise intensity and a decrease in the wall-normal and spanwise fluctuations.

To determine the details of the fibre-flow interactions suggested by the scatter plots and single point correlations, we consider instantaneous visualizations of the flow field and the correlated fibre quantities. In figure 13 we present a projection of the velocity vectors and contours of normal fibre stress in the plane perpendicular to the flow on the left, and on the right we show contours of the fibre wall-normal force directly affects the flow at the same location along with the velocity. Fibre stress is large near a stagnation region between vortices, and a dipole of fibre body force results from this monopole of stress. The region of positive fibre y-body force is associated with a region in which the velocity vectors point in

the negative y-direction and vice-versa and thus acts to decelerate the surrounding vortices. We observe similar behavior for τ_{33} as shown in figure 14. Again, the largest value of stress is associated with a stagnation region between vortices and gives rise to body forces that oppose the vortex motion. These decelerations in turn weaken vortex structure and disrupt the near-wall vortex generation mechanism responsible for skin friction.

4 Discussion

This work has led to physical explanations of the mechanism of polymer and fibre drag reduction using a multiscale approach in the polymer study.

The joint pdfs presented in Fig. 8a and 8b shows how polymers enhance the streamwise momentum in high speed streaks located around $y^+ = 5$. Polymers are allowed to coil in these regions due to the reduction of turbulent kinetic energy by viscous dissipation as shown in Fig. 8b. Extraction of energy from near-wall vortices by polymers occur as polymers are pulled around the vortices, either by upwash or downwash flows. Using Brownian dynamics simulations, Terrapon *et al.* (2004) showed that polymers experience significant straining around vortices, leading to large stretching. The importance of each transfer of energy for the self-sustained turbulence in drag reduced flows has been established by simple numerical experiments reported in Dubief *et al.* (2004*a*).

Based on these results, we propose to include the effects of polymers in the autonomous regeneration cycle put forward by Jiménez & Pinelli (1999). This cycle, shown in Fig. 15, explains how wall turbulence is self-sustained through mean shear, non-linear interactions, near-wall vortices and streaks, in the Newtonian case. Polymers fit at the center of this cycle by extracting energy from the vortices and releasing energy in the streaks. The stretching of polymers is governed by the mean shear and non-linear interactions as shown in Terrapon *et al.* (2004). This simple mechanism appears to apply to LDR and HDR regime, as a matter of fact, it should apply to any regime where streaks and vortices are present. Fig. 15 also contains a sketch of the different actions of polymers around a vortex. Only the most dramatic phenomena, vortex damping and near-wall high-speed streaks enhancement are highlighted.

For fibres, instantaneous visualizations of the flow field (not shown) show that high stress regions are confined to intervortex regions and are most pronounced in regions of intense vortex activity. These regions disappear when the vortex structures are weakened. The high stresses were found to be caused by strong planar alignment of fibres. We therefore infer that the fibres are reoriented in the flow direction after the vortex structures are weakened. Visualizations of the principal axis of the fibre orientation tensor as a function of time demonstrated that this is the case. Some high stress regions persist even after the vortices are weakened due to the lag in this reorientation process. After the fibres reorient in the flow direction, the reduction in local fibre stress allows the vortices to reemerge and the turbulence is sustained in a weakened state.

5 Important Finds and Conclusion

The present simulations were able to provide extremely valuable insights in polymer dynamics and in the transfer of energy between polymers and turbulence. The numerical method was shown to apply to different geometries (boundary layer) and other additives (fibres). The most important results which led to the models of polymer and fibre drag reduction are listed here:

1. At low *We* rare events of strong biaxial flows cause the chain to unravel (Terrapon *et al.*, 2004).

2. at higher *We* different flow types can stretch the polymer molecule, but only bursts of biaxial extensional flow can fully extend it (Terrapon *et al.*, 2004).

3. Simulations of LDR and HDR regimes were performed(Dubief *et al.*, 2004*b*).

4. Transfer of energy between polymers and turbulence were found to occur in a well-organized manner triggered by coherent turbulent structures(Dubief *et al.*, 2004*b*).

5. Drag reducing and turbulence enhancing effects caused by polymer dynamics were shown to be confined to the near-wall region (Dubief *et al.*, 2004*b*).

6. The mechanism of polymer drag reduction has been described as a modified auto-regeneration cycle of near wall turbulence (Dubief *et al.*, 2004*b*).

7. A new algorithm for the simulation of viscoelastic turbulent boundary layer flow was developed to simulate friction drag reduction of incoming Newtonian turbulence for a homogeneous polymer solution (Dimitropoulos *et al.*, 2003).

8. major viscoelastic effects are located with 20% of the boundary layer thickness (Dimitropoulos *et al.*, 2003).

9. A phase difference between polymer stretch and vortex damping was found to exist and be dependent upon the polymer relaxation time (Dimitropoulos *et al.*, 2003).

10. Drag reduction with fibre additives has the same effect on statistics as polymer additives at LDR.(Paschkewitz *et al.*, 2004).

11. For fibres, elasticity has a negative impact on drag reduction effectiveness(Paschkewitz *et al.*, 2004).

12. Fibres create drag reduction via an extensional mechanism in inter-vortex regions(Paschkewitz *et al.*, 2004).

13. The drag reduction effectiveness of rigid fibres is limited due to requirement of the interaction of multiple vortices for drag reduction to occur. As drag reduction decreases, vortices are weaker and move farther apart(Paschkewitz *et al.*, 2004).

6 Significant Software Development

Three codes were developed and validated during this work: a channel flow code coupled with a Brownian dynamics solver, a channel flow solver for constitutive polymer or fibres models and a boundary layer code for constitutive polymer models. All codes are fully-parallelized.

7 Special Conditions for Further Research

The constitutive polymer model used (FENE-P) did not incorporate internal modes. Since polymers are not significantly stretched at HDR, the lack of internal modes which will increase polymer stress compared to the FENE-P prediction is very is very likely to be responsible for an underestimation of the magnitude of drag reduction. Further effort should be made toward the development of a more complete macroscopic model.

Fibres hold the hope of combining with polymers to produce higher drag reduction as it was suggested by some experiments. The coupling of the two additives' effects is currently investigated.

The physical insights gained by our numerical simulations can be used to derive or assess new macroscopic models for DNS, Large Eddy Simulation (LES) or Reynolds Average Navier Stokes (RANS) simulations.

References

BIRD, R., CURTISS, C., ARMSTRONG, R. & HASSAGER, O. 1987 *Dynamics of Polymer Liquids, Vol. 1, Fluid Mechanics*, 2^{nd} edn. New-York: Wiley.

CHONG, M. S., PERRY, A. E. & CANTWELL, B. J. 1990 A general classification of three-dimensional flow field. *Phys. Fluids A* **2**, 765.

DIMITROPOULOS, C. D., SHAQFEH, E., MOIN, P. & LELE, S. K. 2003 A method for direct numerical simulation of viscoelastic turbulent boundary layer flow. In *Internal CTR report*.

DIMITROPOULOS, C. D., SURESHKUMAR, R., BERIS, A. N. & HANDLER, R. A. 2001 Budget if reynolds stress, kinetic energy and streamwise enstrohpy in viscoelastic turbulent channel flow. *Phys. Fluids* **13** (4), 1016–1027.

DUBIEF, Y. 2002 Direct numerical simulation of polymer flow. In *Annual Research Briefs*, pp. 197–208. Center For Turbulence Research.

DUBIEF, Y., TERRAPON, V. E., WHITE, C. M., SHAQFEH, E. S. G., MOIN, P. & LELE, S. K. 2004*a* New answers on the interaction between polymers and vortices in in turbulent flows. *Flow, Turbulence and Combustion* To appear.

DUBIEF, Y., WHITE, C. M., TERRAPON, V. E., SHAQFEH, E. S. G., MOIN, P. & LELE, S. K. 2004*b* On the coherent drag-reducing and turbulence-enhancing behavior of polymers in wall flows. *J. Fluid Mech.* Submitted.

HERRCHEN, M. & OETTINGER, H. 1997 A detailed comparison of various fene dumbbell models. *J. Non-Newtonian Fluid Mech.* **68**, 17–42.

HINCH, E. & LEAL, L. 1976 Constitutive equations in suspension mechanics. part 2. approximate forms for a suspension of rigid particles affected by brownian rotations. *J. Fluid Mech.* **76**, 187–208.

JACOBS, R. & DURBIN, P. 2001 Simulations of bypass transition. *J. Fluid Mech.* **428**, 185–212.

JIMÉNEZ, J. & MOIN, P. 1991 The minimal flow unit in near-wall turbulence. *J. Fluid Mech.* **225**, 213–240.

JIMÉNEZ, J. & PINELLI, A. 1999 The autonomous cycle of near-wall turbulence. *J. Fluid Mech.* **389**, 335–359.

LUND, T., WU, X. & SQUIRES, K. 1998 Generation of turbulent inflow data for spatially-developing boundary layer simulations. *J. Comp. Phys.* **140**, 233–258.

MIN, T., YOO, J. Y. & CHOI, H. 2001 Effect of spatial discretization schemes on numerical solutions of viscoelastic fluid flows. *J. Non-Newtonian Fluid Mech.* **100**, 27–47.

MIN, T., YOO, J. Y. & CHOI, H. 2003*a* Maximum drag reduction in a turbulent channel flow by polymer additives. *J. Fluid Mech.* **492**, 91–100.

MIN, T., YOO, J. Y., CHOI, H. & JOSEPH, D. D. 2003*b* Drag reduction by polymer additives in a turbulent channel flow. *J. Fluid Mech.* **486**, 213–238.

NA, Y. 1996 Direct numerical simulation of turbulent boundary layers with adverse pressure gradient and separation. PhD thesis, Stanford University.

OETTINGER, H. 1996 *Stochastic Processes in Polymeric Fluids*. Berlin: Springer.

PASCHKEWITZ, J. S., DUBIEF, Y., SHAQFEH, E. S. G. & MOIN, P. 2004 Numerical simulation of turbulent drag reduction using rigid fibres. *J. Fluid Mech.* Submitted.

PIERCE, C. 2001 A progress-variable approach for large-eddy simulation of turbulent combustion. PhD thesis, Stanford University.

PTASINSKI, P. K., BOERSMA, B. J., NIEUWSTADT, F. T. M., HULSEN, M. A., VAN DEN BRULE, B. H. A. A. & HUNT, J. C. R. 2003 Turbulent channel flow near maximum drag reduction: simulations, experiments and mechanisms. *J. Fluid Mech.* **490**, 251–291.

SOMASI, M., KOMAMI, B., WOO, N., HUR, J. & SHAQFEH, E. 2002*a* Brownian dynamics simulations of bead-rod and bead-spring chains: Numerical algorithms and coarse graining issues. *J. Non-Newtonian Fluid Mech.* **108**, 227–255.

SOMASI, M., KOMAMI, B., WOO, N., HUR, J. & SHAQFEH, E. 2002*b* Brownian dynamics simulations of bead-rod and bead-spring chains: Numerical algorithms and coarse graining issues. *J. Non-Newtonian Fluid Mech.* **108**, 227–255.

TERRAPON, V. E., DUBIEF, Y., MOIN, P. & SHAQFEH, E. S. G. 2003 Brownian dynamics simulation in a turbulent channel flow. In *2003 Joint ASME/JSME Fluids Engineeing Symposium on Friction Drag Reduction*. Honolulu, Hawaii, USA.

TERRAPON, V. E., DUBIEF, Y., MOIN, P., SHAQFEH, E. S. G. & LELE, S. K. 2004 Simulated polymer stretch in a turbulent flow using brownian dynamics. *J. Fluid Mech.* To appear.

VIRK, P. S. & MICKLEY, H. S. 1970 The ultimate asymptote and mean flow structures in Tom's phenomenon. *Trans. ASME E: J. Appl. Mech.* **37**, 488–493.

WARHOLIC, M. D., MASSAH, H. & HANRATTY, T. J. 1999 Influence of drag-reducing polymers on turbulence: effects of Reynolds number, concentration and mixing. *Exp. Fluids* **27**, 461–472.

WHITE, C., SOMANDEPALLI, V. & MUNGAL, M. 2003*a* The turbulence structure of drag reduced boundary layer flow. *Exps. Fluids* (in press).

WHITE, C. M., SOMANDEPALLI, V. S. R. & MUNGAL, M. G. 2003*b* The turbulence structure of drag reduced boundary layer flow. *Exp. Fluids* To be published.

Line/symbol	L	$We_{\tau 0} = \frac{\lambda u_{\tau 0}^2}{\nu}$	$We = \frac{\lambda U}{h}$	β	DR
----					0%
○	100	36	3	0.9	35%
●	60	84	7	0.9	47%
■	100	120	10	0.9	60%

Table 1: Polymer parameters used for the viscoelastic simulations. The Weissenberg number $We_{\tau 0}$ is normalized the wall-shear stress for the Newtonian simulation (DR=0%).

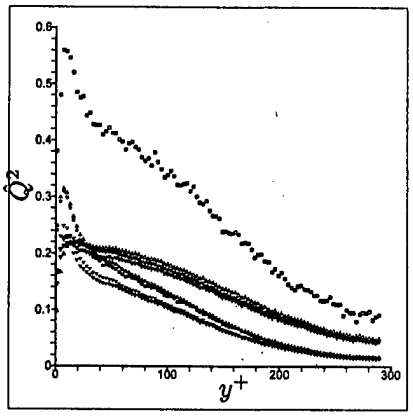

Figure 1: Square extension as a function of the distance to the wall for the four different models. Closed symbol: mean, open symbol: rms. △ : Constitutive FENE-P, □ : Brownian FENE-P, ◁ : FENE, ▽ : Multichain (5 modes) .

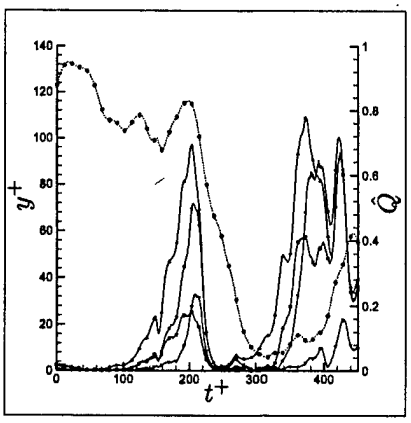

Figure 2: Comparison of the different models along the same trajectory. ○ : y^+, △ : Constitutive FENE-P, □ : Brownian FENE-P, ◁ : FENE, ▽ : Multichain.

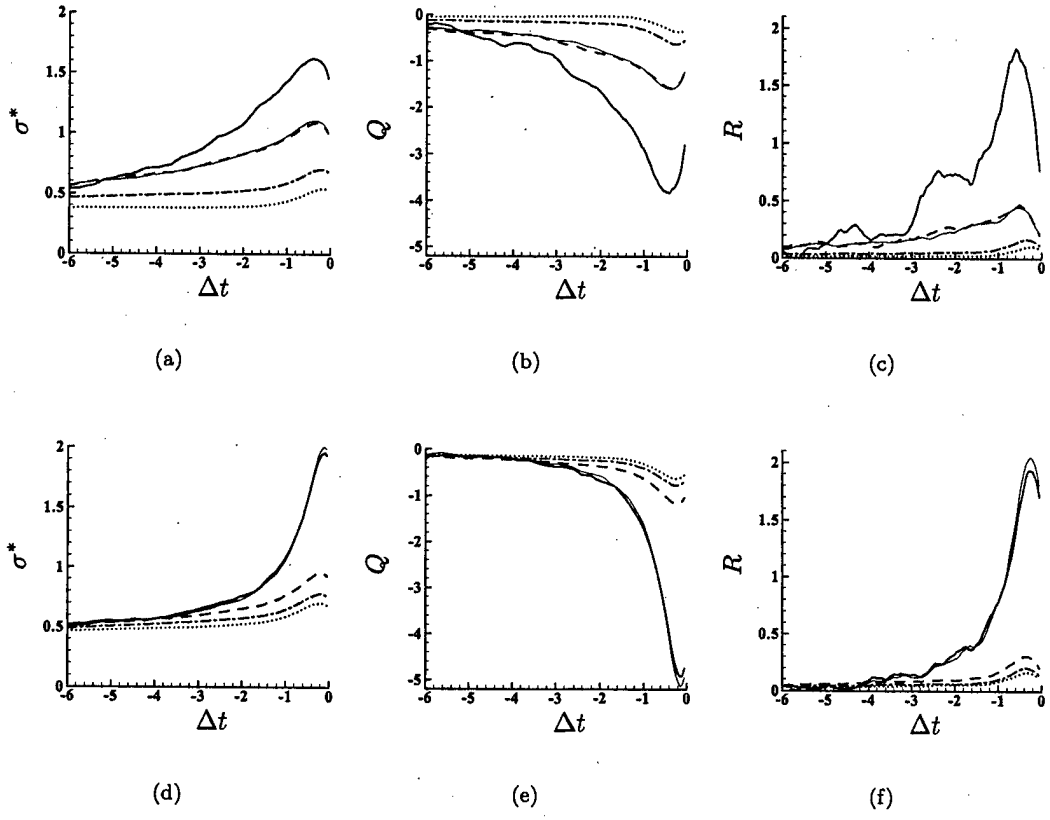

Figure 3: Conditional average of σ^*, Q and R for the polymer molecules crossing the threshold value $q/q_{max} = r$ as a function of the time Δt before crossing this threshold. (a,b,c): $r = 0.65$ and ——, $We = 1.0$; – – –, $We = 1.5$; — · —, $We = 3.0$.; · · · ·, $We = 6.0$. (d,e,f): $We = 3.0$ and ——, $r = 0.95$; – – –, $r = 0.85$; — · —, $r = 0.75$.; · · · ·, $r = 0.65$. Shown for comparison as a thin continuous line: $(a\text{-}c)$ results from a bead-spring chain with $N_b = 11$ beads at $We = 1.5$; $(d\text{-}f)$ results from the FENE-P model for $r = 0.95$.

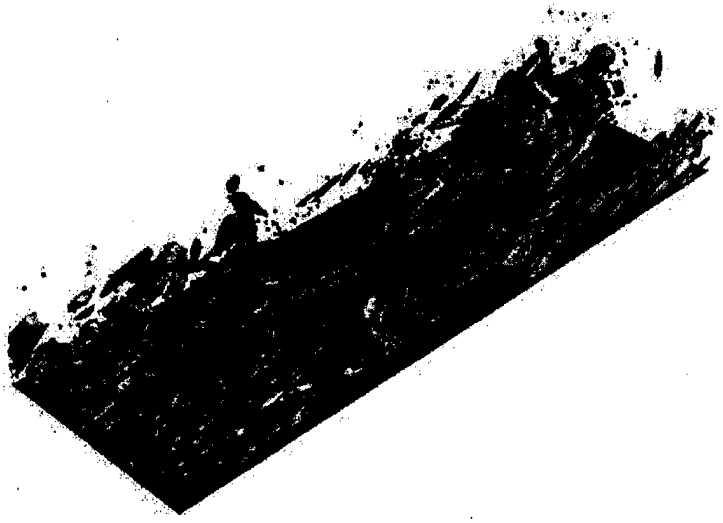

Figure 4: Instantaneous view of the lower half of the channel showing the isosurface $Q = 1.9$ (grey) representing the vortices, the isosurface (turquoise) of $\sigma^* = 1.6$ and the polymer molecules (red) with $q/q_{max} > 0.8$ at $We = 3$.

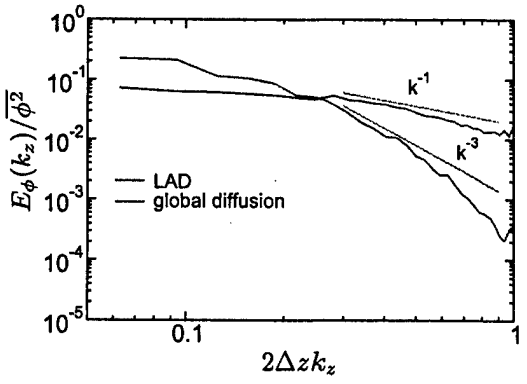

Figure 5: Spectra of polymer stress. Treatment of the advection term in the FENE-P: upwind scheme combined with local artificial dissipation (blue); addition of a dissipative term to the model (red).

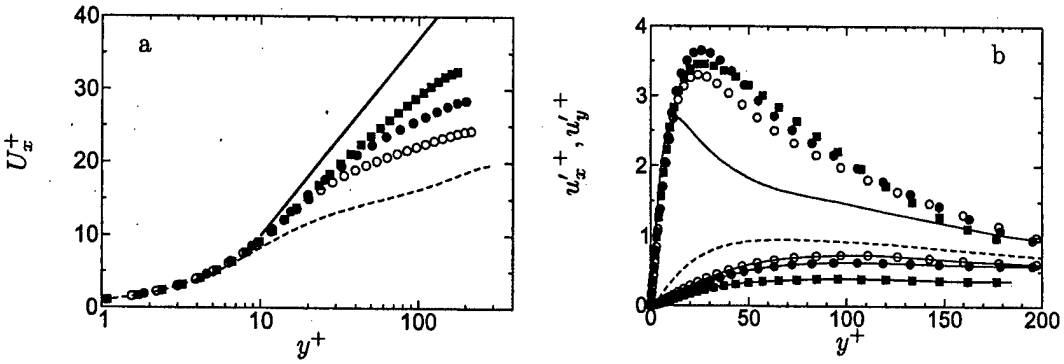

Figure 6: *Left*: Mean velocity profiles scaled with inner variables. —— : MDR asymptote, $U^+ = 11.7 \ln y^+ + 17$. Symbols and lines are defined in Table 1. *Right*: RMS of velocity fluctuations scaled with inner variables. Newtonian simulation (DR=0%): —— , $u_x'^+$; ---- , $u_y'^+$. For the viscoelastic simulations, symbols are defined in Table 1, $u_x'^+$ is denoted by symbols only; $u_y'^+$ is indicated by symbols connected by —— .

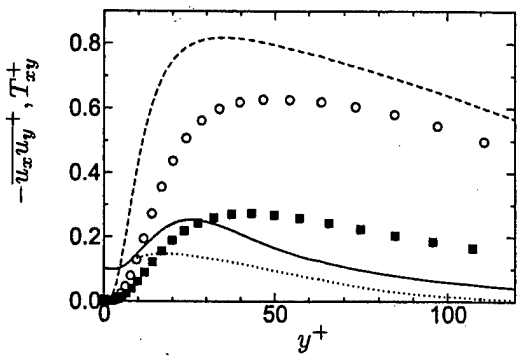

Figure 7: Reynolds shear stress (---- , ○ and ■ as in Tab. 1) and polymer stress (····· : DR=35%, —— : DR=60%) normalized by u_τ and ν. DR=47% is not plotted for clarity.

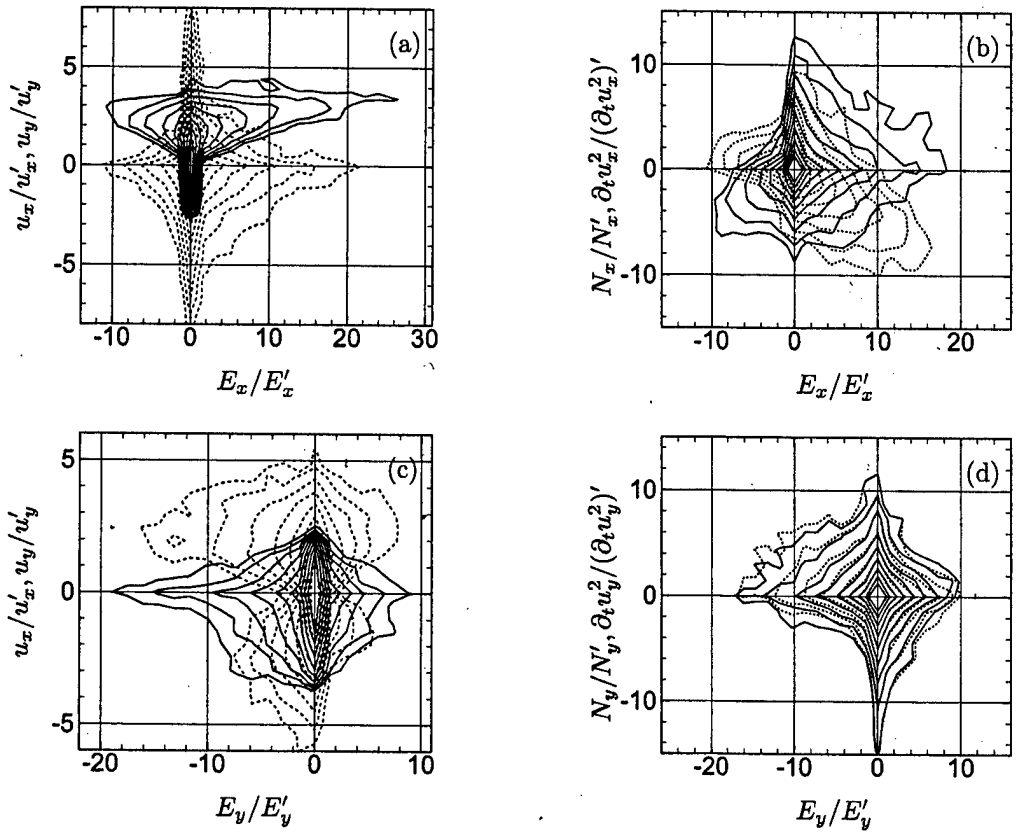

Figure 8: Joint probability density functions of polymer work *vs.* other relevant quantities. For each quantity, fluctuations are normalized by the respective standard deviation. Only data at DR=60% is shown. Fig. a: E_x *vs.* u_x (———) and u_y (----) at $y^+ = 5$. Fig. b: E_x *vs.* $N_x = A_x + P_x + V_x$ (----) and $\frac{1}{2}\partial_t u_x^2$ (———) at $y^+ = 5$. Fig. c: E_y *vs.* u_x (———) and u_y (----) at $y^+ = 50$. Fig. d: E_y *vs.* $N_y = A_y + P_y + V_y$ (----) and $\frac{1}{2}\partial_t u_y^2$ (———) at $y^+ = 50$.

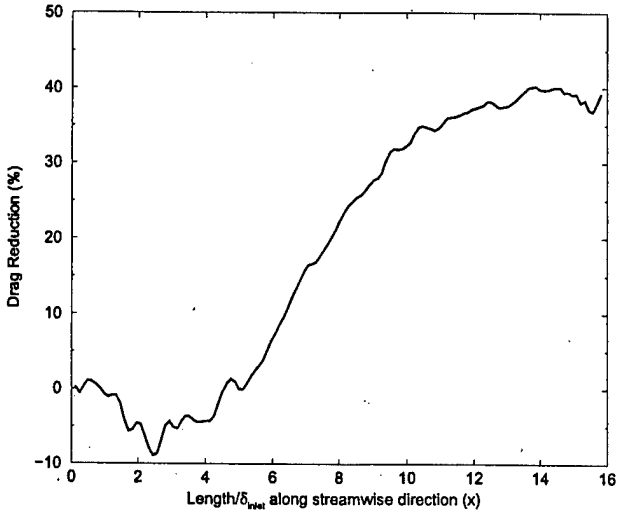

Figure 9: Coupled DNS for $\beta = 0.9$, $Re_\theta = 300$, $L^2 = 3600$ and $We_\tau = 50$: Predicted drag reduction along the streamwise length of the boundary layer.

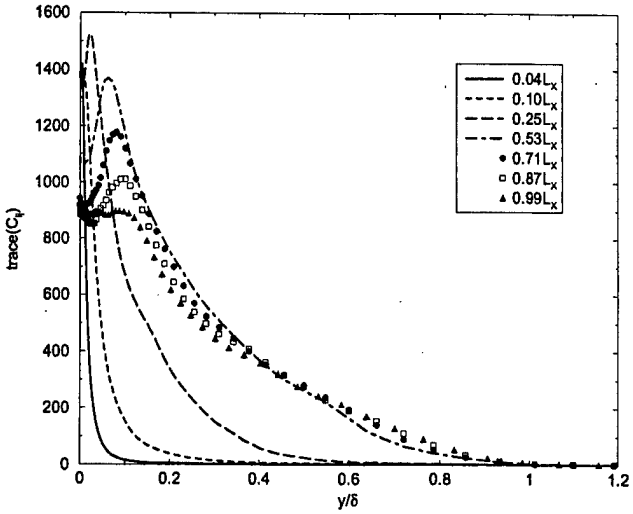

Figure 10: Coupled DNS for $\beta = 0.9$, $Re_\theta = 300$, $L^2 = 3600$ and $We_\tau = 50$: Average polymer extension along the wall normal direction at different locations downstream.

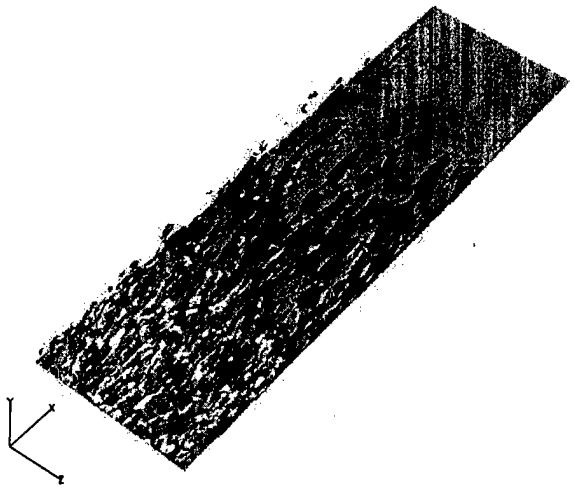

Figure 11: Coupled DNS for $\beta = 0.9$, $Re_\theta = 300$, $L^2 = 3600$ and $We_\tau = 50$: Instantaneous snapshot of the isosurfaces of the second invariant of the velocity gradient tensor with Q=0.075 (grey) and of the trace of the conformation tensor with threshold 1600 (black).

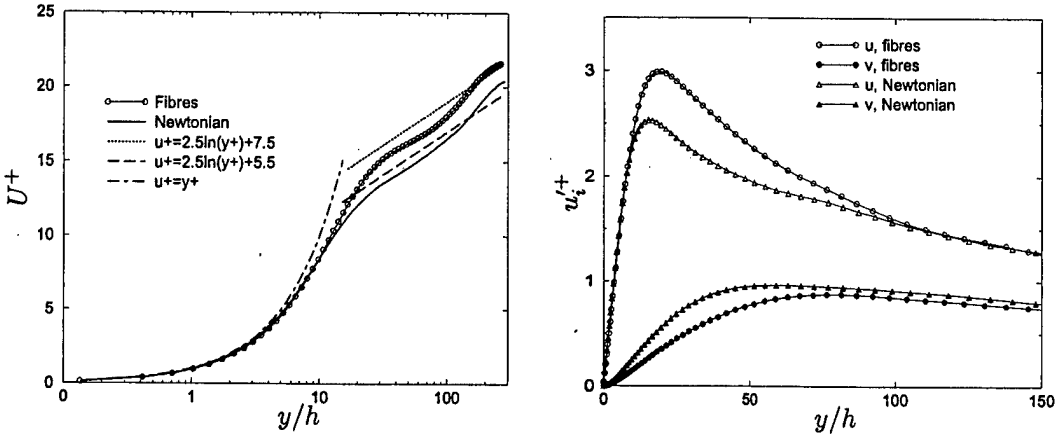

Figure 12: Mean velocity (*left*) and RMS velocity fluctuations (*right*) scaled with friction velocity. Fibre parameters: Pe=1000, aspect ratio=100, $nL^3 = 287$

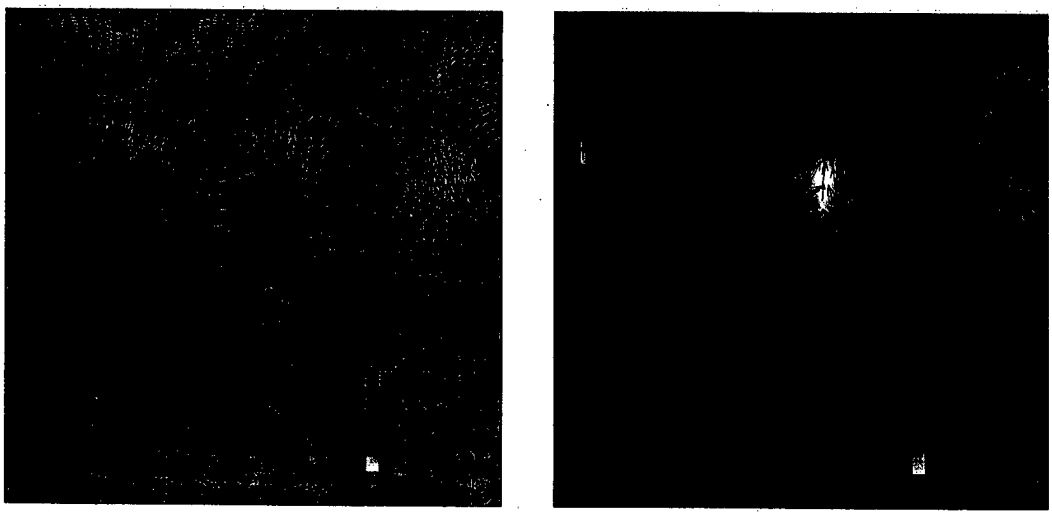

Figure 13: Contours of fibre stress τ_{22} (left) and fibre y-body force (right) with y-z plane projection of velocity vectors

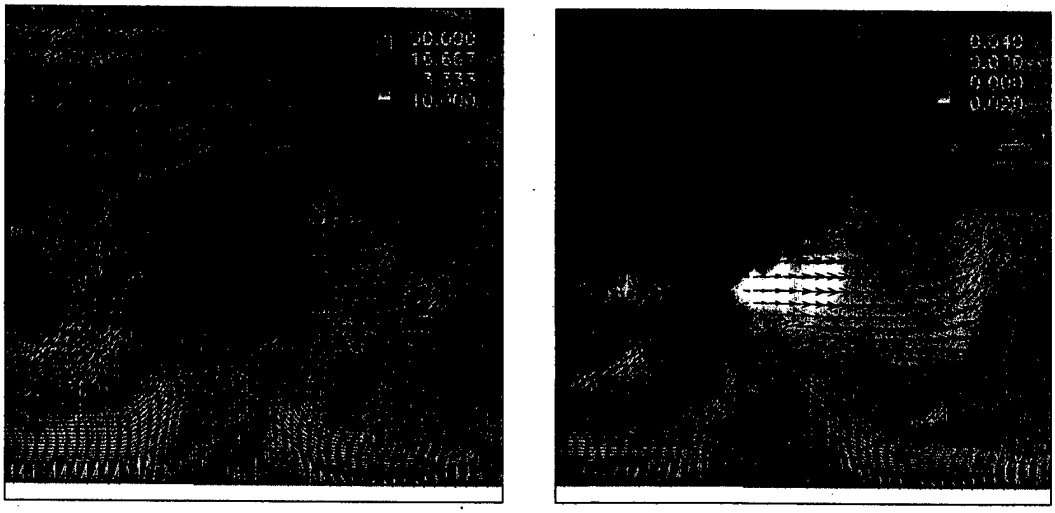

Figure 14: Contours of fibre stress τ_{33} (left) and fibre z-body force (right) with y-z plane projection of velocity vectors

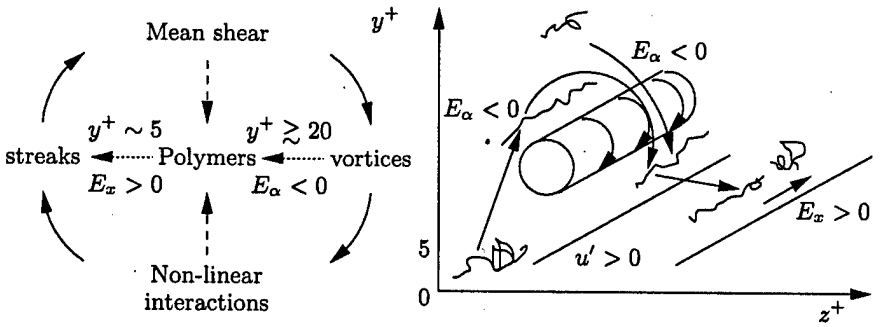

Figure 15: Left: Sketch of the cycle of wall turbulence regeneration with energy transfer from the polymers to the flow and *vice versa*, ····· denotes the action of polymers on turbulence, ---- the main actions of stretching. Right: Vortex pumping fluid from the near-wall region and creating turbulence-damping polymer work and re-injecting stretched polymers into the near-wall region, thereby generating turbulence enhancing polymer work.